Isomeric excitation of ^{235}U by inelastic scattering of low-energy electrons

Boqun Liu and Xu Wang ®*

Graduate School, China Academy of Engineering Physics, Beijing 100193, China

The nucleus of ^{235}U has a low-lying isomeric state of energy about 76.7 eV. Excitation cross sections of the nucleus from the ground state to the isomeric state by inelastic electron scattering are calculated on the level of the Dirac distorted-wave Born approximation. The cross sections are about six orders of magnitude higher than known values based on the Dirac plane-wave Born approximation, emphasizing the vital importance of wave function distortion in the nuclear excitation. In addition, we find that even with low-energy electrons on the order of 100 eV, relativistic effects are significant without which the excitation cross sections drop by an order of magnitude.

I. INTRODUCTION

It has been known since 1957 that the ^{235}U nucleus has a low-lying isomeric state (denoted ^{235m}U) of energy around 76.7 eV above the nuclear ground state [1–5]. The half-life of this isomeric state is about 26 min, decaying almost solely via internal conversion. This isomeric state may be exploited to control nuclear fission, with the thermal-neutron fission cross section for ^{235m}U being about 2.5 times higher than that for the nuclear ground state [6–8]. Proposals have also been made to exploit this isomeric state for isotope separation [9,10].

Besides these potential applications, ^{235}U has been a particularly interesting system to study nucleus-electron couplings, including processes such as nuclear excitation by electron transition (NEET) [9–12], nuclear excitation by electron capture (NEEC) [13,14], and electronic bridge (EB) [15–18]. NEET is associated with bound-bound electronic transitions: The nucleus is excited by the energy released from an electronic transition between a higher bound state and a lower bound state. NEEC is associated with free-bound electronic transitions, and EB is associated with bound-bound electronic transitions in the presence of a laser field, which compensates the energy mismatch between the nuclear transition and the electronic transition. The usage of ^{235}U for the study of nucleus-electron-coupling processes is not surprising, because ^{235m}U is one of the two known nuclear excited states with energy below 1 keV (the other and the lowest nuclear excited state being the isomeric state of ^{229}Th, which has an energy around 8.3 eV [19–23]), and electrons with energies on the order of 10 to 100 eV can be conveniently produced by lasers [24–26].

In addition to the above-mentioned processes, there is another nucleus-electron coupling process, namely, nuclear excitation by inelastic electron scattering (NEIES) [27–29], which is associated with free-free electronic transitions. The nucleus is excited by the energy released from an electronic

transition between a higher continuum state and a lower continuum state. The advantage of NEIES compared to other nucleus-electron coupling processes is that the resonant condition with the nuclear transition can always be fulfilled. In contrast, the resonant condition is rather difficult to fulfill especially for NEET or EB processes.

It is somewhat surprising to find that the NEIES process is largely overlooked in past studies of ^{235}U [30]. Especially for theory, the best that we can find in the literature is an estimation based on a Dirac plane-wave (PW) Born approximation, under which the isomeric excitation rate per nucleus is estimated to be 10^{-16} s^{-1} for a plasma with electron density $n_e = 10^{19}$ cm^{-3} and temperature $T = 100$ eV [31]. This corresponds to an excitation cross section on the order of 10^{-44} cm^2. However, recent studies on ^{229}Th show that special care must be taken for low-energy electrons, especially for the usage of the PW Born approximation [32,33]. Indeed, we show similarly in the current paper that the PW Born approximation is an extremely bad approximation for low electron energies around 100 eV for ^{235}U. It underestimates the excitation cross section by over *6 orders of magnitude*. With the electron wave functions calculated as Dirac distorted waves (DWs) in the current paper, we show that the excitation cross section is on the order of 10^{-38} to 10^{-37} cm^2. The excitation rate per nucleus for the same plasma condition given above is then on the order of 10^{-10} s^{-1}, comparable to or even larger than the competing NEEC process, which is calculated to be on the order of 10^{-11} s^{-1} per nucleus [31].

In addition, we find that relativistic effects are significant even with low-energy electrons on the order of 100 eV. If the electron wave functions are calculated as Schrödinger DWs, the obtained nuclear excitation cross section is an order of magnitude smaller than that obtained with Dirac DWs. This seems rather unintuitive at first glance and is analyzed by comparing the corresponding electron wave functions.

The goal of the current paper is to present and document calculation results on the isomeric excitation cross section of ^{235}U via inelastic scattering of low-energy electrons, for the benefit of future studies or analyses in this research area.

*xwang@gscaep.ac.cn

This paper is organized as follows. In Sec. II we outline the theoretical framework for the calculation. Numerical results and discussions will be given in Sec. III. A conclusion will be given in Sec. IV. Atomic units ($\hbar = m_e = e = 1$) are used throughout this paper unless otherwise stated.

II. THEORETICAL FRAMEWORK

The reaction rate of inelastic electron scattering from the nucleus is given by Fermi's golden rule

$$\Gamma = 2\pi |\langle f| H_I |i\rangle|^2 \rho(E_f), \tag{1}$$

where $\rho(E_f) = p_f E_f/8\pi^3 c^2$ is the density of electron final states, with p_f and $E_f = c\sqrt{p_f^2 + c^2}$ being the momentum and energy of the electron. The state of the whole system is written as the product of the nuclear state $|IM\rangle$ with the quantum numbers I and M, the electron scattering state $|\psi\rangle$, and the photon number state $|n\rangle$:

$$|i\rangle = |I_i M_i\rangle \otimes |\psi_i\rangle \otimes |0\rangle, \tag{2}$$

$$|f\rangle = |I_f M_f\rangle \otimes |\psi_f\rangle \otimes |0\rangle. \tag{3}$$

The interaction Hamiltonian H_I is given by

$$H_I = -\frac{1}{c} \int [\mathbf{J}_n(\mathbf{r}) + \mathbf{J}_e(\mathbf{r})] \mathbf{A}(\mathbf{r}) d\tau$$
$$+ \int \frac{\rho_n(\mathbf{r})\rho_e(\mathbf{r}')}{|\mathbf{r} - \mathbf{r}'|} d\tau d\tau', \tag{4}$$

where $\rho_{n/e}$ and $\mathbf{J}_{n/e}$ are the charge density and current density of the nucleus or the electron, respectively, and $\mathbf{A}(\mathbf{r})$ is the vector potential of the radiation field. The transition matrix element of H_I can be written as [29]

$$\langle f| H_I |i\rangle = \sum_{\lambda\mu} \frac{4\pi}{2\lambda + 1} (-1)^\mu$$
$$\times \left[\langle\psi_f| \mathcal{N}_{\lambda\mu}^E |\psi_i\rangle \langle I_f M_f| \mathcal{M}_{\lambda,-\mu}^E |I_i M_i\rangle \right.$$
$$\left. - \langle\psi_f| \mathcal{N}_{\lambda\mu}^M |\psi_i\rangle \langle I_f M_f| \mathcal{M}_{\lambda,-\mu}^M |I_i M_i\rangle \right], \tag{5}$$

where $\mathcal{N}_{\lambda\mu}^{E/M}$ and $\mathcal{M}_{\lambda\mu}^{E/M}$ are electric (E) or magnetic (M) multipole transition operators with angular quantum number λ and magnetic quantum number μ for the electron and for the nucleus, respectively. They can be written in the following forms:

$$\mathcal{N}_{\lambda\mu}^E = \frac{ik_{\rm is}^\lambda}{c\lambda(2\lambda - 1)!!} \int \mathbf{J}_e(\mathbf{r}) \nabla \times \mathbf{L}[h_\lambda(k_{\rm is}r)Y_{\lambda\mu}(\hat{r})] d\tau,$$

$$\mathcal{N}_{\lambda\mu}^M = \frac{k_{\rm is}^{\lambda+1}}{c\lambda(2\lambda - 1)!!} \int \mathbf{J}_e(\mathbf{r}) \mathbf{L}[h_\lambda(k_{\rm is}r)Y_{\lambda\mu}(\hat{r})] d\tau,$$

$$\mathcal{M}_{\lambda\mu}^E = \frac{(2\lambda + 1)!!}{c(\lambda + 1)k_{\rm is}^{\lambda+1}} \int \mathbf{J}_n(\mathbf{r}) \nabla \times \mathbf{L}[j_\lambda(k_{\rm is}r)Y_{\lambda\mu}(\hat{r})] d\tau,$$

$$\mathcal{M}_{\lambda\mu}^M = \frac{-i(2\lambda + 1)!!}{c(\lambda + 1)k_{\rm is}^\lambda} \int \mathbf{J}_n(\mathbf{r}) \mathbf{L}[j_\lambda(k_{\rm is}r)Y_{\lambda\mu}(\hat{r})] d\tau.$$

In the above formulas, $\mathbf{L}$ is the angular momentum operator, h_λ is the spherical Hankel function, j_λ is the spherical Bessel function, and $Y_{\lambda\mu}$ is the spherical harmonics. $k_{\rm is} = E_{\rm is}/c$ (with $E_{\rm is} = 76.7$ eV) is the wave number corresponding

to the nuclear isomeric transition. According to the selection rule for multipole radiation and parity conservation, the transition from the nuclear ground state to the isomeric state is mainly of type $E3$. Making use of the Wigner-Eckart theorem [34], the differential cross-section of nuclear isomeric excitation can be given as

$$\frac{d\sigma_{E\lambda}}{d\Omega} = \frac{4E_f E_i}{c^4} \frac{p_f}{p_i} \frac{B(E\lambda)}{(2\lambda + 1)^3} \sum_\mu |\langle\psi_f| \mathcal{N}_{\lambda\mu}^E |\psi_i\rangle|^2, \tag{6}$$

where $d\Omega$ is the solid angle of the scattered electron, and $B(E\lambda) \equiv B(E\lambda; I_i \to I_f)$ is the reduced transition probability of the nucleus. For the transition from the ground state to the isomeric state of ^{235}U, $B(E3) = 0.009$ W.u. (Weisskopf units) [18].

In the process of electron inelastic scattering, the electron in the initial and final channels are both continuum states. Dirac DWs are used to describe the electron with momentum **p**, total energy E, direction $\mathbf{v} = \mathbf{p}/p$, and spin v [35]:

$$\psi_{\mathbf{p}v}^{(\pm)} = 4\pi \sqrt{\frac{E + c^2}{2E}}$$
$$\times \sum_{jlm} [\Omega_{jlm}^*(\mathbf{v})\chi_v] e^{\pm i\delta_{jl}} \begin{pmatrix} g_{jl}(r)\Omega_{jlm}(\hat{r}) \\ -if_{jl'}(r)\Omega_{jl'm}(\hat{r}) \end{pmatrix}, \tag{7}$$

where δ_{jl} is the total phase shift of the corresponding partial wave. The electron in the initial (final) state takes the $+$ ($-$) sign. $g_{jl}(r)$ and $f_{jl}(r)$ are radial wave functions for the upper and lower component, respectively. $l' = 2j - l$. Ω_{jlm} are spherical spinors given by

$$\Omega_{jlm}(\hat{r}) = \sum_{v=\pm 1/2} \langle l, 1/2, m - v, v| j, m\rangle Y_{l,m-v}(\hat{r})\chi_v, \tag{8}$$

where the spinor χ_v has the two components

$$\chi_{1/2} = (1, 0)^T, \quad \chi_{-1/2} = (0, 1)^T. \tag{9}$$

The scattering electron feels the potentials from both the nucleus and the atomic electron cloud. These potentials can be determined by first determining the corresponding charge distributions. The distribution of the protons is given by the Fermi distribution [36]

$$\rho_p(r) = \frac{\rho_0}{\exp[(r - R_n)/z] + 1}, \tag{10}$$

where $R_n = 1.07 A_N^{1/3}$ fm with $A_N = 235$ being the nuclear mass number, $z = 0.546$ fm, and ρ_0 is a constant determined by normalization. The density of the atomic electron cloud, denoted $\rho_{\rm el}(r)$, is calculated by a Dirac-Hartree-Fock-Slater self-consistent method [37,38]. The potential energies are then calculated by

$$V_{\rm nuc}(r) = -\int \frac{\rho_p(r')}{|\mathbf{r} - \mathbf{r}'|} d\tau', \tag{11}$$

$$V_{\rm el}(r) = \int \frac{\rho_{\rm el}(r')}{|\mathbf{r} - \mathbf{r}'|} d\tau'. \tag{12}$$

The total potential is $V(r) = V_{\rm nuc}(r) + V_{\rm el}(r)$. Figure 1 shows, for example, $rV(r)$, $rV_{\rm nuc}(r)$, and $rV_{\rm el}(r)$ for the neutral ^{235}U atom.
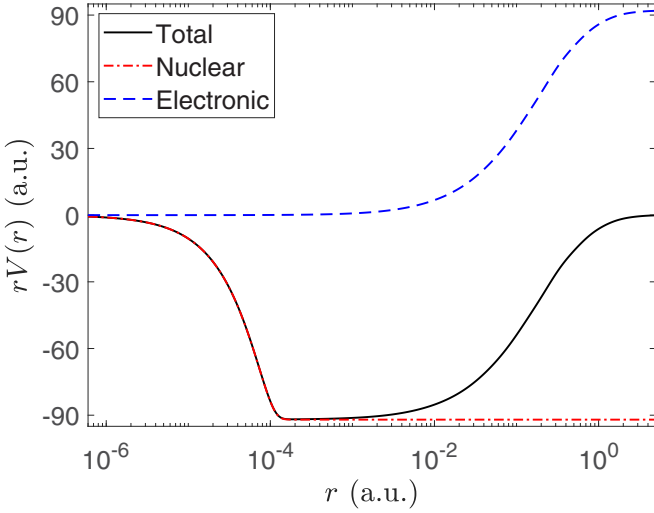
FIG. 1. Black solid curve: The total potential energy felt by the scattering electron from the neutral ^{235}U atom. The red dash-dotted curve shows the potential from the nucleus and the blue dashed curve shows the potential from the electron cloud. Note that the vertical axis gives $rV(r)$ and the horizontal axis is in logarithmic scale.

With the potential $V(r)$, the radial wave functions $g_{jl}(r)$ and $f_{jl}(r)$ in Eq. (7) can be obtained by numerically solving the corresponding time-independent Dirac equation. In the current work the electron radial wave functions are calculated using the code RADIAL [39]. Substituting Eq. (7) into Eq. (6), averaging over the initial states and summing over the final states, and integrating over the electron solid angle, one obtains the total nuclear excitation cross section

$$
\sigma_{E\lambda} = \frac{8\pi^2}{c^4} \frac{E_i + c^2}{p_i^3} \frac{E_f + c^2}{p_f} k_{\text{is}}^{2\lambda+2} B(E\lambda)
$$
$$
\times \sum_{l_i, j_i, l_f, j_f} \frac{(2l_i + 1)(2l_f + 1)(2j_i + 1)(2j_f + 1)}{[(2\lambda + 1)!!]^2}
$$
$$
\times \begin{pmatrix} l_f & l_i & \lambda \\ 0 & 0 & 0 \end{pmatrix}^2 \begin{Bmatrix} l_i & \lambda & l_f \\ j_f & \frac{1}{2} & j_i \end{Bmatrix}^2 |\mathcal{R}_{fi}^{E\lambda}|^2. \quad (13)
$$

The six-component expressions in the parentheses and the curly brackets are the Wigner 3-j and 6-j symbols, respectively. The radial matrix element $\mathcal{R}_{fi}^{E\lambda}$ is calculated as

$$
\mathcal{R}_{fi}^{E\lambda} = \int_0^\infty \Bigg\{ [g_i(r)g_f(r) + f_i(r)f_f(r)]h_\lambda(k_{\text{is}}r)r^2
$$
$$
- [g_i(r)g_f(r) + f_i(r)f_f(r)]h_{\lambda-1}(k_{\text{is}}r)\frac{k_{\text{is}}r^3}{\lambda}
$$
$$
+ [f_f(r)g_i(r) - g_f(r)f_i(r)]h_\lambda(k_{\text{is}}r)k_{\text{is}}r^3 \Bigg\} dr. \quad (14)
$$

Note that the first line in the integral is much larger than the second and the third lines due to the relative strength between the large and the small components of the radial wave functions and the relative strength between $h_\lambda(k_{\text{is}}r)$ and $h_{\lambda-1}(k_{\text{is}}r)$.
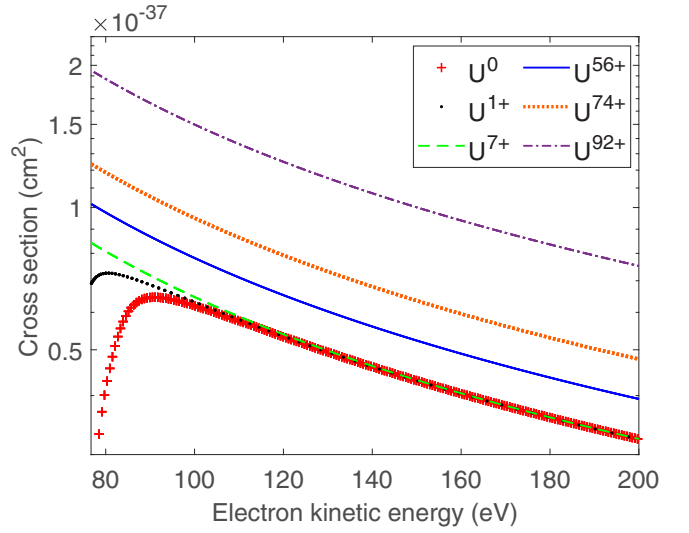

FIG. 2. Isomeric excitation cross sections of ^{235}U by electron inelastic scattering, for several atomic or ionic states as labeled. The excitation energy threshold of ^{235m}U is 76.7 eV.

III. RESULTS AND DISCUSSIONS

A. Isomeric excitation cross sections

Figure 2 shows the nuclear isomeric excitation cross sections by electron inelastic scattering for various atomic or ionic states of ^{235}U, from the neutral atom to the bare nucleus. We are mainly concerned here with low electron energies below 200 eV, which are most relevant to experiments using laser-generated plasmas [9,10,31,40–42].

One can see from Fig. 2 that the cross sections are on the order of 10^{-38} to 10^{-37} cm^2, and the differences between ionic states are not essential: The bare nucleus (U^{92+}) leads to excitation cross sections about 3 to 4 times higher than the neutral atom (U^0). The cross sections show an overall decrease with the increase of electron energy, except for a suppression near the threshold energy of 76.7 eV shown in the U^0 and the U^{1+} cases.

Similar threshold suppression behavior is also seen in the neutral-atom case of ^{229}Th [32,33]. This suppression is due to detailed distortion of the electron wave function by the potential $V(r)$. A simple (or simplistic) understanding would be that for low-energy electrons close to the excitation threshold, penetrating through the electron cloud of a neutral atom is more difficult than penetrating through that of an ion, which has less electrons (hence weaker repulsions).

B. Effect of wave function distortion

If we put the potential energy $V(r) = 0$, then the electron wave function of Eq. (7) reduces to the Dirac PW $|\psi\rangle = |u\rangle e^{i\mathbf{kr}}$ with

$$
|u\rangle = \sqrt{\frac{E + c^2}{2E}} \begin{pmatrix} \chi_\nu \\ \frac{c\hat{\sigma}\hat{p}}{E+c^2}\chi_\nu \end{pmatrix}, \quad (15)
$$

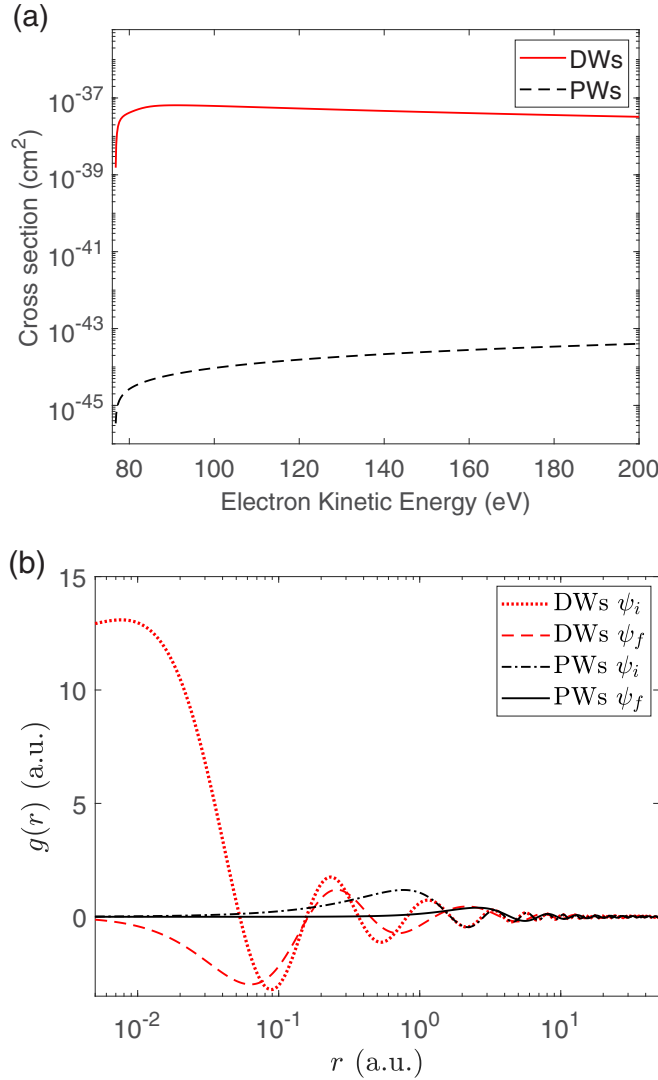where $\hat{\sigma}$ is the Pauli operator.

FIG. 3. (a) Nuclear excitation cross section calculated with Dirac PWs, in comparison to that with Dirac DWs (for the neutral atom). (b) The upper components of the radial wave functions $g(r)$ for $P_{1/2} \rightarrow D_{5/2}$. The kinetic energy of the incident electron is assumed to be 100 eV. Red (gray) curves are for DWs and black curves are for PWs.

The excitation cross section obtained with Dirac PWs is shown in Fig. 3(a), in comparison to that obtained with Dirac DWs. Only the neutral-atom case is shown for the DWs. One can see that the cross section for PWs has magnitudes around 10^{-45} to 10^{-44} cm^2, about 6 to 7 orders of magnitude lower than that for DWs. Therefore wave function distortion has an extremely large effect on the excitation cross section. This discrepancy disqualifies the estimations using PWs [31], although they are most convenient.

The differences in the cross section between PWs and DWs originate, of course, from wave function distortion by the potential $V(r)$. The electron wave functions are distorted such that more population is concentrated in the region that is most efficient for nuclear excitation. This region turns out to be 0.01 a.u. $< r < 0.1$ a.u. from a closer analysis of Eq. (14). Figure 3(b) shows the (large components of) the radial wave

functions that are involved in the $P_{1/2} \rightarrow D_{5/2}$ partial-wave transition for the DW case and for the PW case, with an initial electron energy of 100 eV. One sees that the DWs have much higher amplitudes than PWs in the efficient region for excitation. This difference in the electron wave functions leads to the dramatic differences in the nuclear excitation cross section.

C. Relativistic effect

Even with low electron energies, relativistic effects cannot be neglected for ^{235}U due to the high nuclear charge of $Z = 92$. This point can be demonstrated by calculating the isomeric excitation cross section using Schrödinger DWs:

$$\psi_k^{(\pm)} = \frac{1}{k} \sqrt{\frac{2}{\pi}} \sum_{lm} i^l e^{\pm i \delta_l} g_l(r) Y_{lm}^*(\hat{k}) Y_{lm}(\hat{r}), \quad (16)$$

where δ_l is the total phase shift of the corresponding partial wave. The total excitation cross section for electric multipole transitions is given by

$$\sigma_{E\lambda} = \frac{64\pi^2}{(2\lambda+1)^2} \frac{1}{k_i^3 k_f} B(E\lambda)$$
$$\times \sum_{l_i l_f} (2l_i+1)(2l_f+1) \begin{pmatrix} l_f & l_i & \lambda \\ 0 & 0 & 0 \end{pmatrix}^2 |\mathcal{G}_{fi}^{E\lambda}|^2, \quad (17)$$

where the radial matrix element $\mathcal{G}_{fi}^{E\lambda}$ is calculated as

$$\mathcal{G}_{fi}^{E\lambda} = \int_0^\infty \frac{g_{l_f}(r) g_{l_i}(r)}{r^{\lambda-1}} dr. \quad (18)$$

In Fig. 4(a), we show the comparison of excitation cross sections from Dirac DWs and from Schrödinger DWs, for the neutral ^{235}U atom. (Comparisons of other ionic states give similar results.) It can be seen that the cross section for the Schrödinger case is about an order of magnitude lower than that for the Dirac case, telling the importance of relativistic effects. Note that the small structure shown in the Schrödinger case around 80 eV is due to comparable contributions from two major channels. The partial-wave transition $P \rightarrow D$ drops, whereas the $D \rightarrow P$ transition rises, leading to the small structure in the total cross section.

Similarly, the difference between the Dirac case and the Schrödinger case originates from the difference in the wave functions, especially in the efficient region of 0.01 a.u. $< r < 0.1$ a.u. As shown in Fig. 4(b), the amplitudes of the Schrödinger wave functions are smaller than those of the Dirac wave functions in this region. Furthermore, the main partial-wave contributions to the cross section in the Dirac case are $D_{3/2} \rightarrow P_{1/2}$, $D_{3/2} \rightarrow P_{3/2}$, $D_{5/2} \rightarrow P_{1/2}$, and the corresponding inverse processes. However, in the Schrödinger case, the six channels reduce to two channels ($P \rightarrow D$ and $D \rightarrow P$) due to the neglect of the electron spin. The reduction in the number of channels also leads to a lower excitation cross section in the Schrödinger case.

D. Cross section with higher energies

Seeing the dramatic difference between the excitation cross sections from Dirac PWs and Dirac DWs, it is curious to know
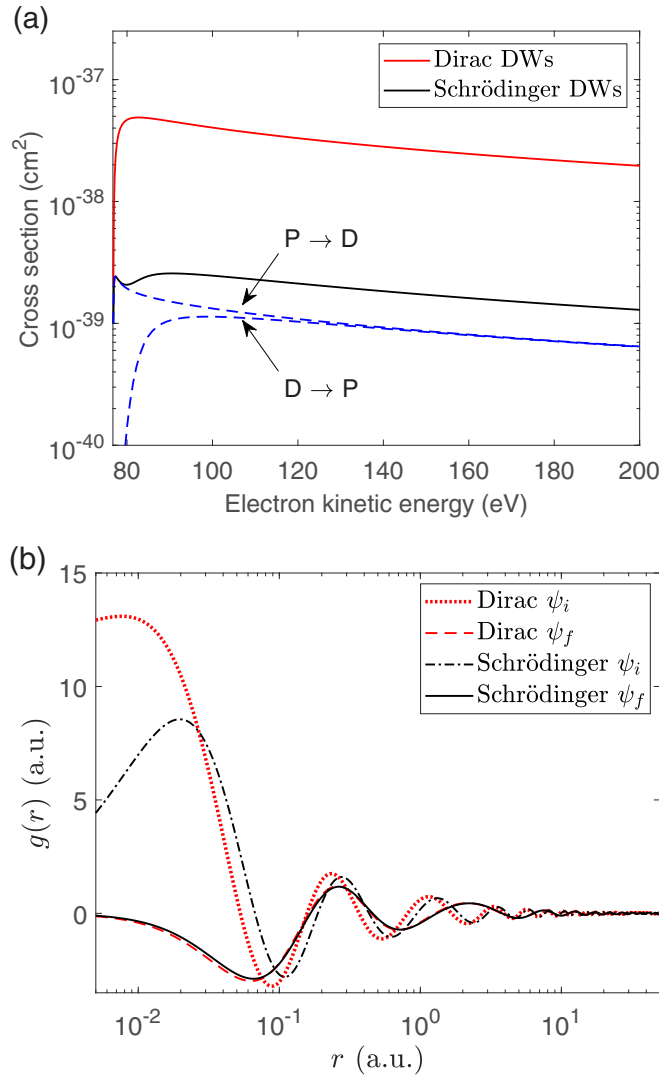
(a)

(b)

FIG. 4. (a) Excitation cross sections calculated using Schrödinger DWs and Dirac DWs, for the neutral-atom case. The blue dashed lines show the two major partial-wave channels for the Schrödinger case. (b) Comparison of relevant radial wave functions. The initial energy of the electron is 100 eV. For the Dirac case, the radial wave functions correspond to the $P_{1/2} \rightarrow D_{5/2}$ transition, and for the Schrödinger case, the radial wave functions correspond to the $P \rightarrow D$ transition.

when the PWs would be good approximations. So we extend the comparison in Fig. 3(a) to a much wider energy range, as shown in Fig. 5. Note that the purpose here is more to fulfill the curiosity, so excitations to higher nuclear levels are not taken into account.

One sees from Fig. 5 that as the electron energy increases, the PW cross section increases monotonically, whereas the DW cross section first decreases (ignoring the small increase just above the threshold) and then increases, with a turning point around 50 keV. The discrepancy between the PW cross section and the DW cross section shrinks with the increase of the electron energy. This is what would be expected, because as the electron becomes faster, the ion-core potential becomes relatively less essential. This tendency being correct, however,
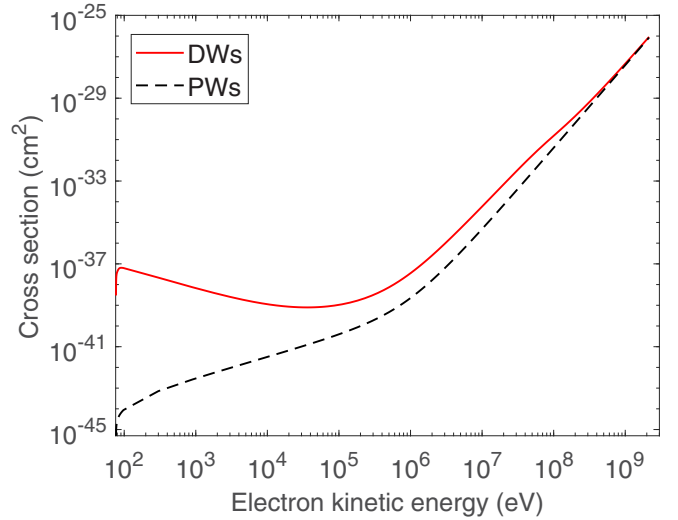

FIG. 5. Same as Fig. 3(a), but in a much larger energy range.

we see that only with very high energies, approaching the order of 1 GeV (10^9 eV), does the PW cross sections agree closely with the DW cross sections.

E. Further remarks

(i) The excitation cross section of 10^{-38} cm^2 is small due to the transition type of $E3$. Yet the excitation may still be detectable. In a laser-generated plasma environment with electron density $n_e = 10^{19}$ cm^{-3} and temperature $T = 100$ eV, we can calculate the excitation rate per nucleus to be $\lambda = n_e \langle \sigma v_e \rangle \approx 10^{-10}$ s^{-1}. The number of excited nuclei is then $N_{\rm exc} = \lambda N t$ with N being the total number of nuclei and t being the excitation time duration. For example, the number of nuclei in 1 gram of ^{235}U is $N = 2.56 \times 10^{21}$. If the total excitation time $t = 1$ s, the number of excited nuclei is $N_{\rm exc} \approx 2.56 \times 10^{11}$ via inelastic electron scattering.

(ii) More efficient excitation from the ground state to the isomeric state may be achieved indirectly via higher excited states. There are several excited states that connect with the ground state by $E2/M1$, or even $E1$, transitions, which may facilitate more efficient population pumping from the ground state. For example, there is a 46.1-keV excited state connecting with the ground state by $E2/M1$ transitions and a 51.7-keV excited state connecting with the ground state by $E1$ transition [43]. Electrons with energies on the order of 100 keV or even higher can also be generated by intense laser pulses [44].

(iii) Our calculations are on the level of the Dirac-Hartree-Fock-Slater self-consistent-field method, which partially takes into account of electron correlations. More sophisticated methods with fuller inclusion of electron correlations [45] may be performed, however, we suspect that the effects of the additional electron correlations are not substantial because the nuclear excitation cross section is rather insensitive to the ion charge state, as shown in Fig. 2. The difference in the excitation cross section between the bare nucleus and the neutral atom is only about 3 times. Were electron

correlations to have a big effect on nuclear excitation, there would be a much more sensitive dependency on the ion charge state.

IV. CONCLUSION

The low-lying nuclear isomeric state of ^{235}U has attracted continuous research attention due to its potential applications as well as intriguing nucleus-electron coupling processes of physical interest. In this paper we focus on one of the nucleus-electron coupling processes, namely, nuclear excitation by inelastic electron scattering. We report calculations of the isomeric excitation cross section on the level of the Dirac distorted-wave Born approximation. We find that the excitation cross sections are over 6 orders of magnitude larger than the previously known values based on the Dirac plane-wave Born approximation. This

nucleus-electron coupling process, therefore, has largely been underestimated.

Detailed analyses are made on factors that affect the excitation cross section, including wave function distortion by the ion-core potential and relativistic effects. We find that wave function distortion plays a crucial role in affecting the nuclear excitation cross section, resulting in the large discrepancy between distorted-wave cross sections and plane-wave cross sections. Besides, somewhat unexpectedly, relativistic effects are found to be rather important even with low electron energies. Our results should be useful for future experiments or theoretical analyses in this research area.

[1] J. R. Huizenga, C. L. Rao, and D. W. Engelkemeir, Phys. Rev. **107**, 319 (1957).

[2] M. S. Freedman, F. T. Porter, F. Wagner, and P. Day, Phys. Rev. **108**, 836 (1957).

[3] V. I. Zhudov, A. G. Zelenov, V. M. Kulakov, V. I. Mostovoi, and B. V. Odinov, JETP Lett. **30**, 516 (1979).

[4] E. Browne and J. K. Tuli, Nucl. Data Sheets **122**, 205 (2014).

[5] F. Ponce, E. Swanberg, J. Burke, R. Henderson, and S. Friedrich, Phys. Rev. C **97**, 054310 (2018).

[6] V. I. Mostovoi and G. I. Ustroev, At. Energ. **57**, 692 (1984).

[7] A. D'Eer, C. Wagemans, M. Néve de Mévergnies, F. Gönnenwein, P. Geltenbort, M. S. Moore, and J. Pauwels, Phys. Rev. C **38**, 1270 (1988).

[8] J. E. Lynn and A. C. Hayes, Phys. Rev. C **67**, 014607 (2003).

[9] M. Morita, PTEP **49**, 1574 (1973).

[10] K. Okamoto, J. Nucl. Sci. Technol. **14**, 762 (1977).

[11] E. V. Tkalya, Nucl. Phys. A **539**, 209 (1992).

[12] E. V. Tkalya, Sov. Phys. JETP **75**, 200 (1992).

[13] V. I. Goldanskii and V. A. Namiot, Sov. J. Nucl. Phys. **33**, 169 (1981).

[14] N. Cue, J. C. Poizat, and J. Remillieux, Europhys. Lett. **8**, 19 (1989).

[15] E. V. Tkalya, Sov. Phys. Dokl. **35**, 1069 (1990).

[16] D. Hinneburg, M. Nagel, and G. Brunner, Z. Phys. A **291**, 113 (1979).

[17] D. Hinneburg, Z. Phys. A **300**, 129 (1981).

[18] J. C. Berengut, Phys. Rev. Lett. **121**, 253002 (2018).

[19] L. A. Kroger and C. W. Reich, Nucl. Phys. A **259**, 29 (1976).

[20] C. W. Reich and R. G. Helmer, Phys. Rev. Lett. **64**, 271 (1990).

[21] R. G. Helmer and C. W. Reich, Phys. Rev. C **49**, 1845 (1994).

[22] B. R. Beck, J. A. Becker, P. Beiersdorfer, G. V. Brown, K. J. Moody, J. B. Wilhelmy, F. S. Porter, C. A. Kilbourne, and R. L. Kelley, Phys. Rev. Lett. **98**, 142501 (2007).

[23] B. Seiferle *et al.*, Nature (London) **573**, 243 (2019).

[24] W. Wang, J. Zhou, B. Liu, and X. Wang, Phys. Rev. Lett. **127**, 052501 (2021).

[25] W. Wang, H. Zhang, and X. Wang, J. Phys. B **54**, 244001 (2021).

[26] X. Wang, Phys. Rev. C **106**, 024606 (2022).

[27] J. A. Thie, C. J. Mullin, and E. Guth, Phys. Rev. **87**, 962 (1952).

[28] L. I. Schiff, Phys. Rev. **96**, 765 (1954).

[29] K. Alder, A. Bohr, T. Huus, B. Mottelson, and A. Winther, Rev. Mod. Phys. **30**, 353 (1958).

[30] R. V. Arutyunyan, L. A. Bol'Shov, V. D. Vikharev, S. A. Dorshakov, V. A. Kornilo, A. A. Krivolapov, V. P. Smirnov, and E. V. Tkalya, Sov. J. Nucl. Phys. **53**, 23 (1991).

[31] M. R. Harston and J. F. Chemin, Phys. Rev. C **59**, 2462 (1999).

[32] E. V. Tkalya, Phys. Rev. Lett. **124**, 242501 (2020).

[33] H. Zhang, W. Wang, and X. Wang, Phys. Rev. C **106**, 044604 (2022).

[34] A. Bohr and B. R. Mottelson, *Nuclear Structure* (Benjamin, New York, 1969), Vol. I.

[35] M. Rose, *Relativistic Electron Theory* (Wiley, New York, 1961).

[36] B. Hahn, D. G. Ravenhall, and R. Hofstadter, Phys. Rev. **101**, 1131 (1956).

[37] D. A. Liberman, D. T. Cromer, and J. T. Waber, Comput. Phys. Commun. **2**, 107 (1971).

[38] J. C. Slater, Phys. Rev. **81**, 385 (1951).

[39] F. Salvat and J. M. Fernandez-Varea, Comput. Phys. Commun. **240**, 165 (2019).

[40] Y. Izawa and C. Yamanaka, Phys. Lett. B **88**, 59 (1979).

[41] C. Granja, J. Kuba, A. Haiduk, and O. Renner, Nucl. Phys. A **784**, 1 (2007).

[42] P. A. Chodash, J. T. Harke, E. B. Norman, S. C. Wilks, R. J. Casperson, S. E. Fisher, K. S. Holliday, J. R. Jeffries, and M. A. Wakeling, Phys. Rev. C **93**, 034610 (2016).

[43] E. V. Tkalya, JETP Lett. **53**, 463 (1991).

[44] J. Feng *et al.*, Phys. Rev. Lett. **128**, 052501 (2022).

[45] E. V. Tkalya, Laser Phys. **14**, 360 (2004).